A program végrehajtásának részletei:

Tekintve, hogy a program két jelentős részének publikálása idénre várható, kérem, hogy a jelentésben foglaltak alapján született minősítést az OTKA kiegészítő eljárásban később, a megjelentetni kívánt közlemények megjelenését figyelembe véve módosítsa.

A program során az alább ismertetett főbb eredményeken túlmenően vizsgálni kívántam, hogy állatok ultrahanggal történő helymeghatározására milyen hatással vannak az esetleges préda állatok által keltett örvények. Az előzetes feltevés szerint denevérek és például delfinek messziről nem elsősorban a kiszemelt prédát "látják" meg ultrahangos érzékelőik segítségével, hanem az azok által keltett örvényeket, amelyek lényegesen nagyobb kiterjedésűek lehetnek a prédánál magánál és esetleges magyarázatot adhatna arra az eddig nem értett jelenségre, hogy miként kapják el azon kis testű állatokat az Echolokalizációval "látó" állatok, melyek mérete az ultrahangos érzékelés felbontása alá esnek.

Ezt a vizsgálatot azonban két oknál fogva nem tudtam a rendelkezésre álló idő alatt befejezni. Egyrészt a szükséges ultrahangos eszközök ára meghaladta azt a mértéket, amit a pályázatból finanszírozni lehetett volna. A többi vizsgált problémához nem volt szükség ekkora finanszírozáshoz, ezért a pénzügyi beszámolóban feltüntetett, körülbelül 1 millió forint visszautalásra is került az OTKA felé.

A fenti problémát egy esetleges együttműködéssel még át lehetett volna hidalni. Azonban az a hallgató, aki a biológiai részekben segített volna elment az egyetemről, így ez a rész nem került megvalósításra, az erre szánt jelentős összeg az OTKA felé visszautalásra is került.

Annyit érdemes még megjegyezni, hogy idén jelentkezett egy doktorandusz, aki denevérek vizsgálatából írja doktoriját, és témavezetője egyetértésével és támogatásával szívesen segít ezen probléma megoldásában. Így reményeim szerint –igaz immár OTKA-m lezárása után- de vissza fogok tudni térni ehhez az érdekes problémához.

Főbb eredmények ismertetése:

1. A tervezett új kísérleti módszer kidolgozása megtörtént. A megoldandó probléma az volt, hogy miként lehet egy analitikusan előre nem ismert, kizárólag csak digitalizált koordinátái révén ismert görbe hosszát a lehető legpontosabban megmérni. Ez ugyanis tipikus helyzet kísérleti adatok elemzésénél. A módszer kidolgozása körökre történt meg, de a kör analitikus tulajdonságainak ismerete csak az eljárás ellenőrzése érdekében került felhasználásra.

Egy digitalizált görbén azt értjük, hogy a görbét alkotó, egymással szomszédságban levő képpontok (X,Y) koordinátái az egész számok halmazán képződnek. Általános tévhit, hogy amennyiben ezen szomszédos képpontok távolságait összeadjuk, akkor a felbontás - ami megadja, hogy a kép karakterisztikus mérete, mint pl. az átmérő mennyi pixelből áll - növelésével az eredmény tetszőleges pontosságúvá tehető.

Mérésekkel bemutatásra került, hogy ez nem így van. Amennyiben a felbontás kicsi, a relatív hiba oszcillál egy felső és egy alsó határ között. A felső határ csökkenő módon konvergál az alsóhoz, amely konstans, de nem zéró. Egységnyi pixel méret mellett a kör átmérőjét növelve és a fenti "naiv" módon történő méréssel a relatív hiba tehát nem nullához, hanem a mérések szerint 5.4 százalékhoz konvergál, azaz a kerület mért értéke hozzávetőleg 1.054-szorosa az adott átmérőhöz tartozó elméleti értéknek és ez az eltérés nem magyarázható azzal, hogy a kör koordinátái milyen módon lettek digitalizálva vagy meghatározva.

A hiba értéke kis felbontások mellett akár 17% is lehet, de az oszcilláció azt jelenti, hogy az átmérőnek vannak olyan "mágikus" értékei, ahol a naiv mérés kis átmérők esetén is a végtelen felbontásnak megfelelő pontosságot adja. Erre azért érdemes felfigyelni, mert amennyiben a naiv módszer alkalmazása történik, célszerű csak ezen mágikus átmérőjű köröknél méréseket végezni.

Egyszerű megfontolások alapján kiszámolható, hogy négyzetrácson a naiv módon mért kerület 8*(SQRT(2)-1) -szerese az elméleti értéknek, ami egyenértékű azzal, mintha a Pi értékére 3,3137 értéket kapnánk, ami megfelel a mérések során kapott 5.4 százalékos relatív hibának.

A fenti eltérés oka az, hogy alakzatok pontos méréséhez nem csak a képpontok közti távolságnak kell egyre kisebb értékhez tartania, de az eltérő egyenes szakaszok meredekségei közti különbségnek is. Utóbbi nem biztosítható, ha a mérés során csak az oldallal illetve sarokkal érintkező szomszédokat vesszük figyelembe, hiszen ezek meredekségei közti különbség csak 45 fokonként változik. Ha egy képpont (pixel) távolságát nem a szomszédjához, hanem egy szomszédot átugorva a szomszéd szomszédjához mérjük, akkor a lehetséges meredekségek száma nő. Általában igaz, hogy N szomszéd átugrásával a lehetséges meredekségek száma N-vel nő, a meredekség diszkrét mivoltából adódó hiba 1/N szerint csökken. Ugyanakkor, ha a vizsgált vonal görbületi sugara kisebb N-nél, akkor egy másik hiba lép be, nevezetesen az, hogy egy görbe szakaszt egyenessel helyettesítünk. Ez a hiba pedig N szerint nő.

Ebből következik, hogy adott görbe esetén a fenti két hiba együttes minimalizálása adja azt az N értéket, ahol a mérés a lehető legpontosabb. Ezen optimális N meghatározására két módszert is megadtunk. Az egyik azt használja ki, hogy az 1/N csökkenés sokkal gyorsabb, mint a korábban említett oszcilláció, ezért az 1/N hiba által dominált tartományban az oszcilláció nem figyelhető meg a mért hosszaknál. Amikor azonban abban a tartományban van N értéke, ahol a görbületek kiegyenesítése okozza a domináló hibát, akkor az oszcilláció már a hossz mérésében is megjelenik (nem csak a relatív hibában). Az optimális N érték tehát ott van, ahol először jelenik meg a mérésben oszcilláció, mert ott van a crossover a két hibajelenség között.

A másik módszer szerint N függvényében elvégezve a különböző méréseket, a kis N tartományra 1/x jellegű, a nagy N tartományára –x jellegű görbét illesztve a crossover helye megtalálható. A mérési eredmények azt mutatják, hogy körökre az optimális N értéke monoton, de nagyon lassan növekvő függvénye az átmérőnek.

Előfordulhat, hogy a crossover nem létezik, mivel például az adott felbontás mellett túl nagy görbületek fordulnak elő. A fent leírt módszer ekkor is fontos üzenetet hordoz: azt, hogy a crossover hiányában a kísérletet esetleg célszerű megismételni más optikai nagyítás mellett, mert a jelenlegi paraméterekkel nincs lehetőség az optimális kiértékelésre.

Egy jellemző példa, ha homogén turbulens jellegű áramlásoknál a sebességek abszolút értékének eloszlását vizsgáljuk. A fentiek értelmében a különböző abszolút értékű sebesség vektorok különböző hibát hordoznak, ami önmagában is befolyásolhatja a hibát figyelembe nem vevő eloszlásfüggvényt. A bevezetett módszer segítségével ez a probléma kiküszöbölhető, mert a kísérletet többször megismételve mindig csak az optimális N mellett mért értékeket vesszük figyelembe, és az ezen értékek mellett kapott eredményekből határozzuk meg a sebességek eloszlását.

Végezetül érdemes megemlíteni, hogy a fenti módszert számítógépes programok részeként alkalmazva gazdasági hasznot is hozhat.

2. Kvázi kétdimenziós áramlások során a nem egyensúlyi rendszerek érdekes skálázást mutatnak Az egyik ilyen jól ismert rendszer az, ahol zajos környezetben (pl. porózus anyag) áramlik a folyadék Az ilyen rendszereket leíró egyenlet a kontextustól függően vagy a Kardar-Parisi-Zhang (KPZ) egyenlet, vagy a véletlenszerű hajtóerőt tartalmazó Burgers egyenlet. Ezek egymásba át is transzformálhatóak.

A probléma kísérleti vizsgálatára rendelkezésre álló lehetőségek viszonylag szűkösek. Az adott esetben szűrőpapírban terjedő folyadék front és szűrőpapír lassú (láng nélküli) égésével létrejövő front mozgását vizsgáltuk. Az új, lényeges vonása ezeknek a vizsgálatoknak az volt, hogy a front terjedését perturbáció mellett vizsgáltuk.

Ismert, hogy egy rendszernek valamilyen perturbációra adott válasza jellemzi a rendszert és hasznos információkra deríthet fényt. Geológiai kutatások során például (pillanatszerű) robbantások okozta lökéshullámok, matematikában a Green függvények olyan módszerek, amelyek a rendszernek a pontszerű perturbációra adott válaszából nyernek információt. Hasonló gondolat tükröződött Wolf és Tang munkájában is, akik kimutatták, ha a felület feldurvulása során egy lokalizált pontban megváltoztatjuk a sebességet, akkor a rendszer válaszából milyen extra információk nyerhetők ki a nem-linearitásra vonatkozóan. Az elv lényege a KPZ esetben egyszerű: ha ugyanolyan mértékű pozitív és negatív perturbációt alkalmazunk, akkor lineáris dinamika esetében a kialakuló átlagos profilok szimmetrikusak a vízszinteshez képest. Ha viszont nem-lineáris dinamika jellemzi a rendszert, akkor a sebesség hasonló mértékű, de ellentétes előjelű perturbálása a vízszinteshez képest anizotróp átlagos profilokat alakít ki.

A fenti gondolat kísérleti felhasználásához porózus anyagban (lencse papír) lokálisan megváltoztattuk a front terjedési sebességét. Folyadék terjedésénél erre két módszert alkalmaztunk. Az elsőnél a papír nedvesítési tulajdonságát változtattuk meg a front terjedésével párhuzamos irányban kémiai eljárás útján. A második esetben egy, a

papírhoz közel tartott vékony huzal segítségével extra kapilláris erőt biztosítottunk helyileg, s ezzel segítettük elő a front terjedését. A második esetben a front terjedésének gátlását a huzal felmelegítésével lehetett elérni, ugyanis ekkor helyileg a párolgás miatt a front retardált lesz.

Hasonló módon a lassú égéssel terjedő front sebességét is tudtuk lokálisan perturbálni. Ekkor kálium nitráttal volt a papír egy csík mentén preparálva. Inverz esetben hasonló koncentrációjú oldattal volt preparálva az egész felület egyetlen, központi csík kivételével. Ez felelt meg az azonos mértékű, de ellentétes előjelű perturbációknak.

A felület profilok átlagát videokamerával felvett számos kép számítógépes kiértékelésével kaptuk meg. Az átlagot kivonva a képeket kiátlagoltuk. Mivel nagyobb kálium-nitrát koncentráció elősegíti a terjedést, a felület teljes átlagsebessége is nő, de a perturbáció természetes módon kiszélesedik, hiszen a középső, előrefutó rész húzza magával az elmaradó széleket. Bár nem várható, hogy a sebesség függése a KN koncentrációtól lineáris (különösen nem az a pinning átmenet közelében), de a vizsgált sebesség tartományban mégis jó közelítéssel szolgált egy lineáris ansatz.

A következőkben követve Wolf és Tang számítását és feltételezve, hogy a felület dinamikája eleget tesz a KPZ egyenlet nem-lineáris verziójának, elvégeztük az egyenlet szétcsatolását az átlagos front terjedését és az átlagos front körüli fluktuációkat leíró tagokra. Az átlagos frontra vonatkozó egyenletet illesztettük a kísérletileg meghatározott átlagos profilokra, hogy az egyenletben szereplő ismeretlen konstansok értékeit meghatározhassuk. (Itt érdemes megjegyezni, hogy ez az eljárás a lineáris esetre is érvényes, hiszen ebben az esetben a nem-lineáris tagok szorzótényezőjére közel nulla értéket várhatunk.)

Így a nem-lineáris tag szorzótényezőjére azt találtuk, hogy karakterisztikusan különbözik zérótól, értéke 5.6 mm/s. A szokásosan “effektív felületi feszültségnek” nevezett lineáris tag szorzótényezőjére pedig 144 mm2/s adódott. A fenti mérést elvégeztük a KN koncentráció kontraszt különböző értékei mellett. Azt tapasztaltuk, hogy a perturbáció helyén és a széleken mért átlagos magasságok különbsége hozzávetőleg négyzetesen nő a KN koncentráció kontraszt értékével.

Effect of a columnar defect on the shape of slow-combustion fronts

M. Myllys, J. Maunuksela, J. Merikoski, and J. Timonen
Department of Physics, University of Jyväskylä, P.O. Box 35, Jyväskylä FIN-40014, Finland

V. K. Horváth
Department of Biological Physics, Eötvös University, 1117 Budapest, Hungary

M. Ha and M. den Nijs
Department of Physics, University of Washington, Seattle, Washington 98195, USA
(Received 7 July 2003; published 7 November 2003)

We report experimental results for the behavior of slow-combustion fronts in the presence of a columnar defect with enhanced or reduced driving, and compare them with those of mean-field theory. We also compare them with simulation results for an analogous problem of driven flow of particles with hard-core repulsion (ASEP) and a single defect bond with a different hopping probability. The difference in the shape of the front profiles for enhanced vs reduced driving in the defect clearly demonstrates the existence of a Kardar-Parisi-Zhang-type nonlinear term in the effective evolution equation for the slow-combustion fronts. We also find that slow-combustion fronts display a faceted form for large enough enhanced driving, and that there is a corresponding increase then in the average front speed. This increase in the average front speed disappears at a nonzero enhanced driving in agreement with the simulated behavior of the ASEP model.

DOI: 10.1103/PhysRevE.68.051103 PACS number(s): 05.40.−a, 64.60.Ht, 05.70.Ln

I. INTRODUCTION

Nonequilibrium interfaces that display interesting scaling properties are quite common in physical (crystal growth, fluid penetration into porous media, etc.), chemical (reaction fronts) as well as biological (growing bacterial colonies) systems. The dynamics of these systems have long been thought to be generically described by the Kardar-Parisi-Zhang (KPZ) equation [1], or some other equation of motion in the same universality class [2]. In two space dimensions in particular (one-dimensional interfaces) when exact solutions are available, the scaling properties of the KPZ equation are well understood. The same is not, however, true for the experimental observations of scaling of interfaces. Typically, one has found a roughening exponent clearly higher than that for the KPZ equation [2]. Various explanations have been suggested as for why the KPZ scaling has not generally been found, and most of the time correlated and/or non-Gaussian noise have been the prime suspects [2,3].

Recent experiments on slow-combustion fronts propagating in paper [4,5], and on flux fronts penetrating a high-T_c thin-film superconductor [6], have provided new insight into this problem [7]. It indeed appears that short-range-correlated noise, quenched and dynamical, with possibly at the same time a non-Gaussian amplitude distribution for small time differences induces an additional length and a related time scale, beyond which KPZ scaling can only be observed. Despite these recent advances, it would still be worthwhile to demonstrate the existence of the nonlinear term, as introduced by Kardar, Parisi, and Zhang [1,8], and essential for the KPZ dynamics, directly from the observed fronts. This would in essence prove that KPZ type of dynamics, including possibly effects of nontrivial noise, can indeed be expected to be generic for nonequilibrium interfaces. One can demonstrate the presence of this term indirectly by using, e.g., inverse schemes able to infer the (partial) differential equation that governs the observed stochastic evolution of interfaces [9], but there is also a way to produce a directly observable effect on the shape of the interface due to this term.

This method for observing the operation of the nonlinear term was suggested already some time ago by Wolf and Tang [10]. They considered the effect of columnar defects, columnar in two space dimensions on which case we concentrate here, and found that there is a clear ''asymmetry'' between the shapes of the fronts that propagate in the presence of a defect with enhanced and correspondingly reduced driving. This asymmetry is a direct consequence of the nonlinear term in the KPZ equation. For a positive coefficient in this term, applicable to slow-combustion fronts, the noise-averaged front should be faceted with a forward-pointing triangular shape around a defect with enhanced driving, with a height proportional asymptotically to the width of the sample in the case of a defect in the middle of the sample, or to the basic period in the case of periodic boundary conditions. In the case of reduced driving in the defect, the shape of the front should not be faceted, and the magnitude of the (negative) deformation in the profile should be proportional, according to this mean-field theory, to the logarithm of the basic period. Despite its apparent simplicity, this kind of experiment has never been performed.

As is well known, the body-centered solid-on-solid interface model in which the nearest-neighbor heights are restricted to differing only by ± 1, displays KPZ behavior, and is on the other hand equivalent to a driven flow of particles (hopping rate p) with hard-core repulsive interactions (ASEP) [2]. A columnar defect in an interface model corresponds to a fixed slow or fast bond (hopping rate rp with $r<1$ or $r>1$, respectively) in the ASEP model. A faceted interface corresponds to a traffic jam of infinite length in the

 ©2003 The American Physical Society

thermodynamic limit behind the slow bond. Another related question is the detailed shape of the density/interface profile. The mean-field theory of Ref. [10] predicts an infinite queue for all $r<1$ and a logarithmic decay of density forwards the average in the depletion zone behind the fast bond for $r>1$, i.e., $r_c=1$. Janowsky and Lebowitz [11] considered the totally asymmetric ASEP model with a slow bond, but concentrated mainly on the shock wave fluctuations far away from the slow bond, and apparently did not consider the faceting/queueing transition (they had a phase diagram with $r_c=1$). The same model was also considered by Kolomeisky [12], but he did not consider the faceting/queueing transition either.

Kandel and Mukamel considered a somewhat different model, which is supposed to be in the same universality class, and proposed [13] that the faceting/queueing transition should take place at a $r_c<1$. Their simulation data were not, however, conclusive.

The ''slow-bond issue'' has also been considered in the context of the directed polymer problem [14–19]. As discussed above, the (1+1)-dimensional ASEP is equivalent to (1+1)-dimensional KPZ-type growth, and the latter to a directed polymer in two dimensions subject to a random potential. The slow bond transforms into a columnar defect with an attractive short-range interaction, and the queueing transition translates into whether the polymer becomes localized to this defect. A number of arguments suggest that the ASEP model is at the critical dimension above which localization takes place at a nonzero strength of the defect, and one thus expects that $r_c=1$ and that the transition likely involves an essential singularity [14–19].

In slow-combustion experiments the detailed shape of the front profile is difficult to determine, and thereby also the disappearance of faceting. Faceting is, however, related to increased front speed, also in the thermodynamic limit, and this is an easier observable. For possible nonfaceted fronts, which would correspond to $r_c<r<1$, an increased front speed would only be a finite-size effect, as also the decreased front speed in the case of a defect with reduced driving corresponding to $r>1$. Notice that the effective nonlinear term is positive in the slow-combustion experiments, while it is negative in the ASEP models. Therefore, enhanced (reduced) driving in the defect in the first case corresponds to a slow (fast) bond in the latter case.

II. EXPERIMENTAL DETAILS

The equipment we use in slow-combustion experiments has been described elsewhere [4,5], so it suffices to say here that samples were ''burned'' in a chamber with controllable conditions and that the video signal of propagating fronts was compressed and stored online in a computer. The spatial resolution of the setup was 120 μm, and the time resolution was 0.1 s. For the samples we used the lens-paper grade (Whatman) which we have also used previously [5]. Lens paper was now used to speed up the experiments.

As slow-combustion fronts do not propagate in paper without adding an oxygen source for maintaining the chemical reaction involved, we added as before [4,5] a small amount of potassium nitrate in the samples. This method also allows for a relatively easy way to produce enhanced or reduced driving in the columnar defect. By using masks it is straightforward to produce a narrow (vertical) stripe with reduced or enhanced amount of potassium nitrate. The average concentration of potassium nitrate determines the average speed of the fronts, so it serves as the control parameter of the problem.

It is, however, quite difficult to accurately regulate the amount of potassium nitrate absorbed in the sample. This means that it is difficult to produce samples with exactly the same base concentration, and the same concentration difference between the base paper and the columnar defect. Therefore, the statistics we get for any fixed difference in the concentration is not quite as good as we would hope. They are adequate for the main features of the fronts but not for such details as, e.g., accurate forms of the front profiles. They are also good enough for a quantitative analysis of changes in the front speed.

The samples were typically 20 cm (width)$\times$40 cm, and the columnar defect (vertical stripe) in the middle of the sample was 1.0 cm wide. The defect cannot be too in our case narrow as fluctuations in the slow-combustion process would then tend to wipe out its effect. Too wide a stripe would on the other hand cause effects due to its nonzero width, which are unwarranted. We also used simulations with a discretized KPZ equation to check that the ratio 1 cm to 20 cm should not cause additional effects [20]. The length of the samples was in most cases adequate for achieving stationary behavior, and only those results are used here where saturation of the profile was evident.

When analyzing the front profiles, the stripe was removed from the data, as well as about 6 mm from both boundaries of the samples. As the system is symmetric across the stripe in the middle, the observed front profiles were also symmetrized for better statistics.

As already reported before [4,5], fluctuations in the slow-combustion fronts in paper are noticeable. For extreme values of the potassium-nitrate concentration there appear problems with pinning (low concentration) or local avalanche type of bursts (high concentration) in the fronts. Also, very small values of the concentration difference between the base paper and the defect stripe could not be used, as fluctuations then completely masked the effect of the defect. These problems were noticeable for reduced driving in the defect in particular. In the data reported here, concentration varied between 0.265 and 0.61 $\mathrm{g\,m^{-2}}$ in the base paper, between 0.1 and 1.05 $\mathrm{g\,m^{-2}}$ in the stripe, and the concentration difference varied between 0.06 and 0.49 $\mathrm{g\,m^{-2}}$ on the positive side (25 burns), and -0.197 and -0.478 $\mathrm{g\,m^{-2}}$ on the negative side (19 burns). Because of the practical restrictions and fluctuation effects, the number of successful burns was relatively small.

III. RESULTS

We will need the dependence on potassium-nitrate concentration of the front velocity below so we consider it first.

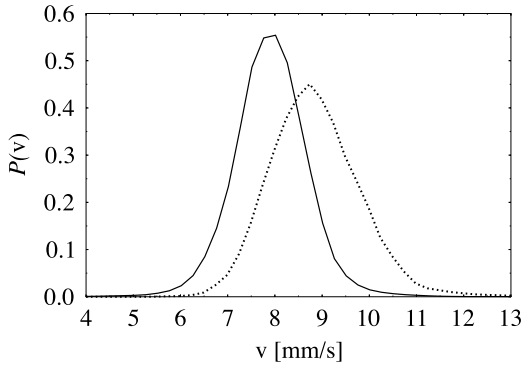

FIG. 1. Velocity distributions for slow-combustion fronts with potassium-nitrate concentrations 0.34 $g\,m^{-2}$ (full line) and 0.536 $g\,m^{-2}$ (dashed line). Velocities are determined for a time difference of 2 s.

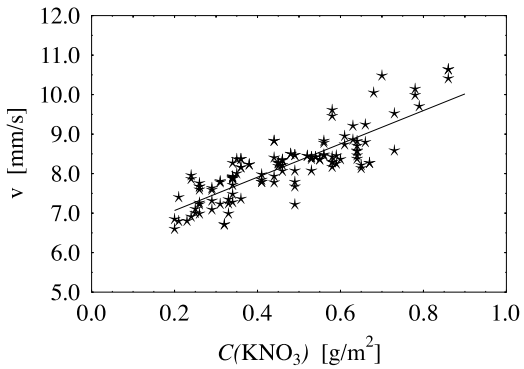

FIG. 2. Front velocity as a function of potassium-nitrate concentration. Measured points are denoted by stars and the line is a linear fit to these points.

It is useful to begin with a discussion of the accuracy of the front-velocity determination.

A. Front velocity

Lens paper is thin so that variations in its mass density and dynamical effects such as (possibly turbulent) convection around the combustion front are both expected to make a contribution to the effective noise. Noise amplitude is consequently relatively large [4,5], and therefore also velocity distribution of a propagating front can be expected to be broad. We show in Fig. 1 the distribution for two different values of the potassium-nitrate concentration.

It is evident from this figure that even though the average velocities in these two cases are relatively well separated and easily distinguishable, the velocity distributions have a big overlap. Together with the limited statistics for any fixed value of (the difference in) the potassium-nitrate concentration, these broad distributions mean that some variation can be expected to occur in the measured average velocities (velocity differences) of the fronts.

In the presence of a columnar defect, we should, e.g., determine the change in the average front speed arising from the defect. This can be accomplished by analyzing separately the undeformed ''flat'' part of the fronts, and the part of the front profile affected by the presence of the defect. Determination of the average speed of the flat fronts is done in the transient (with respect to profile shape) phase in which the (growing) width of the deformed profile is still less than the width of the sample. In this phase the flat part of the front is already in the saturated regime with constant average velocity. The average speed of the deformed profile is determined in a later phase in which the width of the deformed part of the profile essentially coincides with the sample width.

We have also determined the average front velocity for 122 individual burns for a fairly broad interval in the potassium-nitrate concentration, and these data are shown in Fig. 2 together with a linear fit to the measured points.

The dependence on potassium-nitrate concentration of the front velocity is not expected to be linear especially near the pinning limit, but, for the concentration range shown here, it is well approximated by a linear behavior, which is also more convenient for the subsequent analysis. We find that with a linear fit to the data, the front velocity v is given, on average, by

$$v = 4.2C + 6.2, \tag{1}$$

where C is the potassium-nitrate concentration, and v is in units $mm\,s^{-1}$ when C is expressed in $g\,m^{-2}$.

Before showing the measured front profiles in the presence of a columnar defect, let us consider, in order to make later comparisons more transparent, what is expected from the mean-field solution as reported in Ref. [10].

B. Mean-field prediction

We assume that the time evolution of the front $h(x,t)$ is governed by the KPZ equation $\partial h/\partial t = \nu\nabla^2 h + (\lambda/2)(\nabla h)^2 + \kappa + \eta(x,t)$, where $\eta(x,t)$ describes white noise with δ-function correlations in space and time, and the driving term contains the idealized defect as a δ-function contribution, $\kappa = \kappa_0 + \kappa_1 \Sigma_n \delta(x - L/2 + nL)$. For simplicity we assume here as in Ref. [10] periodic boundary conditions. If we average over noise in the KPZ equation and denote $H(x,t) \equiv \langle h(x,t) \rangle$, we find that

$$\frac{\partial H(x,t)}{\partial t} = \nu H'' + \frac{\lambda}{2}(H')^2 + \frac{\lambda}{2}\langle(\nabla\,\delta h)^2\rangle + \kappa, \tag{2}$$

are $H' \equiv H'(x,t)$ denotes the spatial derivative of H and $\delta h \equiv h(x,t) - H(x,t)$ describes fluctuations around the noise-averaged profile. A corresponding equation can be derived for δh [10].

As δh should not depend (locally) on $H(x,t)$ nor on $H'(x,t)$, and only local interdependence between δh and the noise-averaged profile can be assumed to appear, one would then expect [10] that in leading order $\langle(\nabla\,\delta h)^2\rangle = a_0 + a_2 H''(x,t)$, with a_0 and a_2 some constants. This assumption will make Eq. (2) closed so that it can be solved without further reference to the fluctuations. The δ-function contribution in the driving term will induce cusps in $H(x)$ at $x = L/2 - nL$, and the solution of Eq. (2) is therefore equivalent to solving the equation

$$\frac{\partial H(x,t)}{\partial t} = \nu_e H'' + \frac{\lambda}{2}(H')^2 + \kappa_e \tag{3}$$

in the interval $-L/2 \leqslant x \leqslant L/2$, with boundary conditions $H(L/2) = H(-L/2)$ and $H'(\pm L/2) = \pm s$. Here we have defined the effective (renormalized) parameters $\nu_e \equiv \nu + \lambda a_2/2$ and $\kappa_e \equiv \kappa_0 + \lambda a_0/2$, and the magnitude of the slope of the front at the defects is $s \equiv \kappa_1/2\nu_e$.

Equation (3) is the well-known Burgers equation [21] which can be solved in closed form in one space dimension. It is useful to express it first in dimensionless form, which can be achieved with transformations $H = H_0\tilde{H}, x = H_0\tilde{x}/s$, $t = 2H_0\tilde{t}/(\lambda s^2)$, with $H_0 \equiv 2\nu_e/\lambda$ the internal length scale of the system.

We look for a stationary solution of this equation in the form $\tilde{H}(\tilde{x},\tilde{t}) = [\kappa_e + \mathrm{sgn}(\kappa_1)q^2]\tilde{t} + \ln[f(q\tilde{x})]$, where $\mathrm{sgn}(z)$ is the sign of z, and we have already used the Hopf transformation in the spatial part of the ansatz to remove the nonlinearity from the equation for f. We find that [10]

$$f(z) = \cosh(z), \quad q \tanh\left(\frac{q\tilde{L}}{2}\right) = 1 \tag{4}$$

for enhanced driving in the defect ($\kappa_1 > 0$), and

$$f(z) = \cos(z), \quad q \tan\left(\frac{q\tilde{L}}{2}\right) = 1 \tag{5}$$

for reduced driving in the defect ($\kappa_1 < 0$). Here $\tilde{L} \equiv sL/H_0$ is the dimensionless width of the system and $z \equiv q\tilde{x}$. Asymptotically, for $\tilde{L} \gg 1$ (and $\lambda > 0$), the profile around a defect with enhanced driving is a forward-pointing triangle with sides that have slopes $\pm s$ and with height $\Delta H_+ \equiv H(L/2) - H(0) \simeq sL/2$. The asymptotic profile around a defect with reduced driving is given by $H_0 \ln|\cos(\pi x/L)|$ so that $\Delta H_- \simeq -H_0 \ln(sL/\pi H_0)$. The magnitude of H_+ thus grows linearly with L (or s) while that of H_- only grows logarithmically with L (or s). This asymmetry is a direct consequence of the nonlinear term that enhances the deformation in the former case but reduces it in the latter case.

C. Measured front profiles

In the above mean-field theory, $\delta v \equiv \kappa_1/L$ is the difference between the front velocity (driving) inside the defect and outside the defect. In the slow-combustion experiments this velocity difference is regulated by the potassium-nitrate concentration so that now $\delta v = 4.2\Delta C$, where the numerical factor comes from the linear fit given by Eq. (1), and $\Delta C \equiv C_{\mathrm{defect}} - C_{\mathrm{base}}$ is the concentration difference. This means that the scaling factor s is given by $s = 4.2L|\Delta C|/\nu_e$. Without as yet knowing the actual value of ν_e needed for evaluating the size of s and H_0, reasonable estimates, based on the results from the inverse method solution for the effective equation of motion [9], indicate that the slow-combustion fronts are not necessarily in the strictly asymptotic regime: we expect that $\tilde{L} > 1$ but not by a very big margin. Notice that the size of $\tilde{L}$ is now regulated by ΔC as the width L of the samples is held fixed. Despite the achievable values of $\tilde{L}$, we can expect to clearly see the asymmetry in the heights of the front profiles for different signs of the concentration difference. In Fig. 3 we show the averaged (and symmetrized) front profiles for $\Delta C = \pm 0.33$.

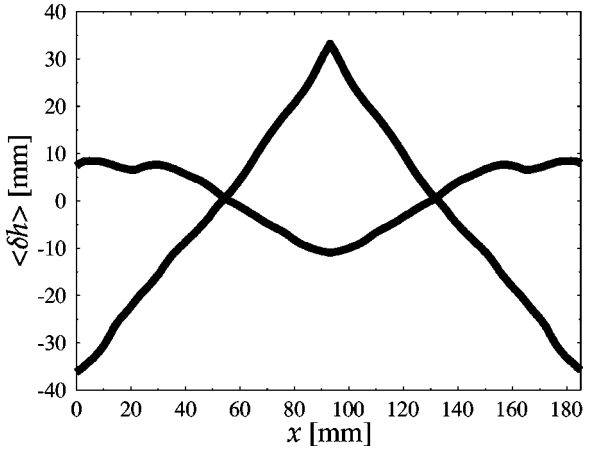

FIG. 3. Average front profiles with a columnar defect for $\Delta C = \pm 0.33$ (upper and lower profiles, respectively).

It is indeed evident that there is a clear difference in the heights of the front profiles around defects with enhanced and correspondingly reduced driving. By following the transient time evolution of the fronts, we could also see a clear difference there. For $\Delta C > 0$, when a triangular deformation was formed after a while around the central stripe, its height and base length grew with a more or less constant velocity until the base length reached the width of the sample, while the slopes of the sides of this triangle remained roughly constant. For $\Delta C < 0$ on the other hand, the height of the deformation saturated much faster even though it also grew more or less linearly in time in the beginning, and the base length of the deformation reached the sample width at the same time. This transient behavior will be analyzed in more detail below. The qualitative behavior for the $\Delta C > 0$ case is clearly visible in Fig. 4 which shows successive fronts with a time difference of 0.5 s for $\Delta C = 0.327$.

A more quantitative comparison between the mean-field solution for the noise-averaged front and the observed slow-combustion fronts can also be made. For this purpose we found it convenient to consider instead of the profile heights $\Delta H_\pm$ the average slopes of the left-hand (LH) sides of the profiles (c.f. Fig. 3), $k_\pm \equiv 2\Delta H_\pm/L$. As we do not expect to be in the strictly asymptotic regime, we have used the full transcendental equations for q in Eqs. (4) and (5) above when fitting the observed $k_\pm$ with the mean-field result.

The average slopes, as functions of concentration difference ΔC, will now depend on two parameters, $A \equiv H_0/L$ and $B \equiv 2.1L/\nu_e$, which are used to fit the measured slopes. From the fitted values for these parameters we can then estimate the coefficients λ and ν_e for this system.

We show in Fig. 5 the experimentally determined values for k_+ and k_- together with the fit by the mean-field solution using Eqs. (4) and (5).

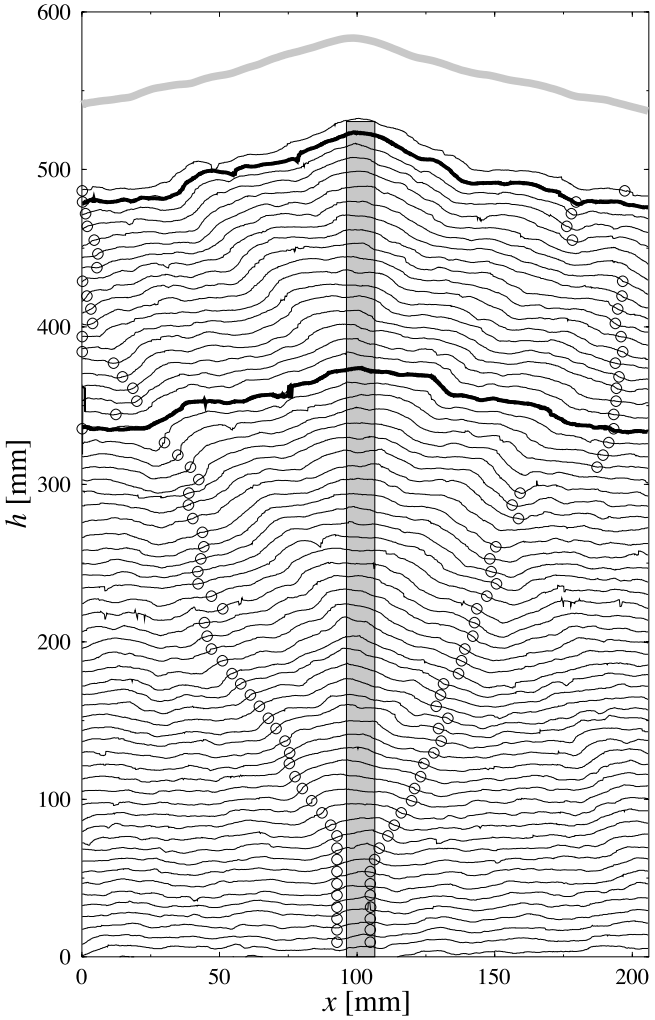

FIG. 4. Successive fronts with a time difference of 0.5 s for the concentration difference $\Delta C=0.327$. Also marked are the stripe with enhanced concentration of potassium nitrate, the fronts between which the average profile is determined (thick lines), the height of the final profile, and the average shape of the profile.

Fits to the data were not very sensitive to the actual value of parameter A so the correlation coefficient did not change much even if A was changed in a relatively large interval. If the $\Delta C>0$ and $\Delta C<0$ data were fitted separately without any restrictions on the two parameters, these fits had also a tendency to produce somewhat different values for the two cases. As the signal-to-noise ratio is better for the $\Delta C>0$ data, we fixed A such that it was between the two separately fitted values but closer to the one from the unrestricted two-parameter fit to the $\Delta C>0$ data, and in the interval within which the quality of this fit was essentially unchanged: $A \simeq 0.3$. Thereafter an unrestricted one-parameter fit to the whole data was used to find the value for B. In this way we found that $B \simeq 2.5$.

The fitted values for parameters A and B allow now an estimation of two physical parameters, the ''renormalized surface tension'' ν_e and the coefficient of the nonlinear term λ. We thus find that $\nu_e \simeq 144\ \mathrm{mm^2\,s^{-1}}$ and $\lambda \simeq 5.6\ \mathrm{mm\,s^{-1}}$. In the estimate for ν_e we used an ''effective'' sample width

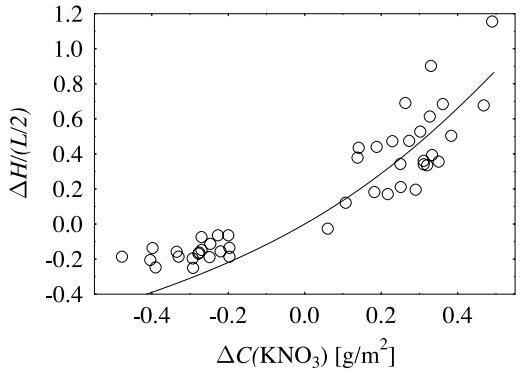

FIG. 5. The absolute value of the average LH slope of the deformed front profile around a columnar defect as a function of difference in the potassium-nitrate concentration. The full line is a fit by the mean-field solution using Eqs. (4) and (5).

$L_{\mathrm{eff}} \simeq 180$ mm, a bit smaller than the width 202 mm of the actual sample, due to the width of the defect stripe and to allowing for some boundary effects. By other methods we have found previously that $\lambda \simeq 4.1$–$5.1\ \mathrm{mm\,s^{-1}}$ [9], so that the value found here is fairly close to these previous estimates.

In view of the unavoidable fluctuations in the measured averaged slopes, we find the fits to the measured points by the mean-field solution to be quite reasonable.

D. Defect-induced change in front velocity and the queueing transition

As already discussed above, the mean-field solution predicts a faceting or queueing transition at $\Delta C=0$. Above this transition ($\Delta C>0$), the average front velocity is increased due to the presence of enhanced driving in the defect, and below this transition the change in front velocity should vanish for large enough $\tilde{L}$. For negative ΔC the change in velocity is negative, and should decrease in magnitude with increasing $|\Delta C|$. According to Kandel and Mukamel [13], this transition should appear at a $\Delta C_{\mathrm{cr}}>0$.

As the numerical data of Ref. [13] are not decisive, and there are other seemingly contradictory results [14–19], we have done [22] simulations on a totally asymmetric ASEP model with a fixed defect bond with hopping rate rp in the middle of the system, while the hopping rate at the other bonds was p. Open boundary conditions were imposed such that the hopping-in rate at the left boundary was αp, and the hopping-out rate at the right boundary was βp. In what follows we only consider the case $\alpha=\beta=p=1/2$.

This model shows [22] a queueing transition at $r=r_c=0.80\pm0.02$. For $r_c<r<1$ there is a power-law shaped density profile around the slow bond, and the profile becomes flat only at $r=1$. For $r>1$, which corresponds to a fast defect bond, the density profile around the defect also displays a power-law shape, but with a different exponent. The density profile thus displays a qualitatively similar difference between a faceted slow-bond case ($r<r_c$) and the corresponding fast defect-bond case as the mean-field solution for the KPZ fronts with enhanced and reduced driving in

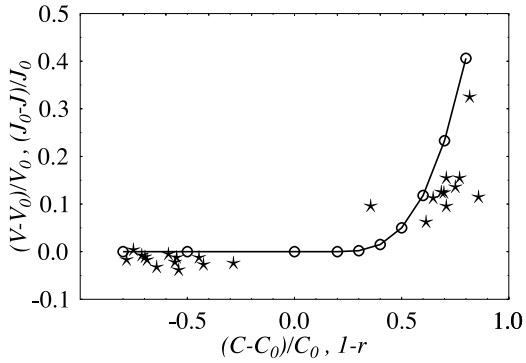

FIG. 6. Scaled velocity change of slow-combustion fronts due to a columnar defect as a function of $(C-C_0)/C_0$ ($\star$), and scaled current change in the totally asymmetric ASEP model due to a defect bond as a function of $(p-rp)/p=1-r$ ($\bigcirc$). The full line connects the latter data points [22].

the columnar defect, respectively, except that in the ASEP solution for a fast defect bond the density profile has a power-law shape instead of a logarithmic one. The mean-field solution does not have a phase that would correspond to that of the power-law shaped density profile around a slow bond in the ASEP model.

Our results thus seem to contradict the directed polymer results [14–19]. One should, however, notice that we find a more complex structure. The queued ASEP phase represents a strongly localized state, while the power-law shaped profile represents a form of weak localization. Earlier directed polymer studies may have been insensitive to this distinction. Support for a weakly localized phase is also reported in Ref. [23]. For more details on the ASEP solution and the transition, see Ref. [22].

As the detailed shapes of the front profiles are difficult to determine experimentally, we only compare the results for the dependence of the average front velocity $V\equiv\langle v\rangle$ (current $J\equiv\langle j\rangle$) on the potassium nitrate concentration C (hopping rate p). In this comparison dimensionless variables are used, $(V-V_0)/V_0$ for the change in the front velocity, and similarly for the current but for reversed sign as enhanced driving in the defect corresponds to a slow bond, $\Delta C/C_0$ for the potassium-nitrate concentration difference, and $\Delta p/p=1-r$ for the hopping-rate difference. Differences are all determined between the value with or at the defect and the value elsewhere or without the defect. In this way no fitting is involved in the comparison. Obviously the actual driving force is not known exactly for the slow-combustion fronts, but the observed linear dependence well above the pinning transition between the potassium-nitrate concentration and the front velocity suggests that the dimensionless difference can be reliably used in this kind of comparison.

This comparison of the slow-combustion experiment and the totally asymmetric ASEP model results is shown in Fig. 6. It is evident from this figure that agreement between the two results is reasonable as there is no fitting involved. There are still fairly large fluctuations in the experimental data, and it is not possible to have results for very small values of ΔC as fluctuations tend to wipe out the whole effect, and the system is then not in the ''asymptotic regime.'' These results

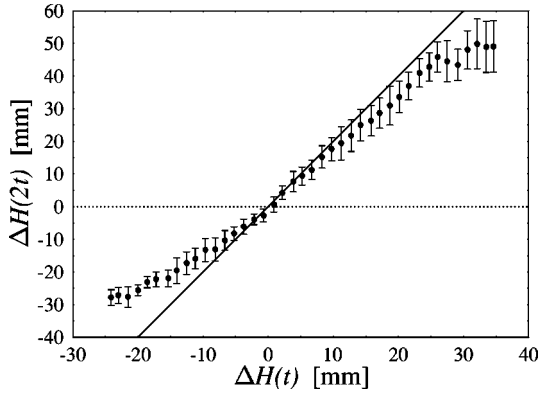

FIG. 7. $\Delta H(2t)$ as a function of $\Delta H(t)$ averaged over 32 burns. Positive values correspond to $\Delta C>0$ and negative values to $\Delta C<0$. The full line is $\Delta H(2t)=2\Delta H(t)$.

indicate, however, that there indeed is a faceting (queueing) transition at a nonzero $\Delta C_{\rm cr}$ (nonzero $\Delta p_{\rm cr}$, i.e., $r_c\neq 1$).

E. Transient behavior

In addition to the stationary profiles analyzed above, it is also possible, as already indicated, to study the transient profiles, i.e., how the defect-induced profiles grow at the initial phases of the process. The transient behavior of the profile around a columnar defect with enhanced driving is particularly simple. The Burgers equation (3) admits in this case a solution of exactly the same shape as the stationary solution, which grows linearly in time until its baseline reaches the width of the sample. Such a ''self-similar'' transient does not exist in the case of negative ΔC, so analytical results for transient behavior are then difficult to find. In the nonasymptotic regime $\tilde{L}\ll 1$ one can, however, show that the situation is symmetric, $\Delta H_-\simeq-\Delta H_+$. One would thus expect that, at least in our case when $\tilde{L}$ is not particularly large, the height $|\Delta H_-|$ would also grow initially (at least nearly) linearly in time.

The expected transient behavior for $\Delta C>0$ is already (qualitatively) evident from Fig. 4 above. More quantitatively the transient time evolution of the height of the deformed profile can be analyzed, e.g., by plotting $\Delta H(2t)$ against $\Delta H(t)$. For a linear time evolution the former value is twice the latter. In Fig. 7 we show this plot, averaged over 32 individual burns, including both signs of ΔC.

The initial transient behavior is approximately linear in time for both cases. For $\Delta C>0$ the trend continues nearly linear until saturation sets in when the width of the profile equals the width of the sample. For $\Delta C<0$ the behavior is quite similar except that saturation takes place earlier. There is also some indication that, in this case, the growth of ΔH becomes nonlinear in time already before saturation, but the quality of the data does not allow for a decisive conclusion on this.

IV. DISCUSSION AND CONCLUSIONS

The difference in the amplitude (height), and perhaps not so clearly in the shape, of the front in the slow-combustion experiments caused by a columnar defect with enhanced or

reduced driving was clearly demonstrated. The behavior of the height of the deformed profile and the qualitative shape of the profile in the case of enhanced driving were also reasonably well explained by the mean-field solution of Ref. [10]. The asymptotic shape of the profile in the case of negative velocity difference could not be unequivocally determined as fluctuations are more important because of relatively small amplitude of the profile in this case. The reduced, in comparison with the case of enhanced driving, height of the profile was very evident. In the case of positive velocity difference, the transient behavior of the profile, i.e., the growth of the defect induced deformation in the profile shape, could as well be explained by the mean-field solution. For negative velocity difference a nearly linear behavior in time was observed initially, followed perhaps by a regime of nonlinear time evolution before saturation.

Fitting the average height (or, equivalently, the average slopes of the sides) of the profile with the mean-field solutions provided us with estimates for the effective surface tension ν_e and the coefficient of the nonlinear term λ. The latter parameter can also be determined from the slope dependence of the local front velocity [5,9], or by applying an inverse method on the observed fronts [9]. The value found here for λ is fairly close to these previous estimates, and we find this level of agreement very reasonable in view of the rather large fluctuations in the present data.

One should, however, notice that the λ measured for a sample depends on the potassium-nitrate concentration in that sample, and that the average potassium-nitrate concentrations were not the same in the samples used in the experiments. We did not take this variation into account, as it can be assumed to give a small effect in comparison with the other experimental uncertainties, so that the present estimate represents an ''average'' value.

The effective surface tension ν_e contains, in addition to the ''bare'' surface tension of the original KPZ equation, an unknown renormalization factor due to noise-induced fluctuations around the average front profile. We cannot thus get an estimate for the bare surface tension ν, which can be estimated by other means [9]. However, we can conclude that the noise-induced renormalization of ν_e appears to be sizable.

The position and nature of the faceting (queueing) transition in interfaces affected by a columnar defect (in the ASEP model by a defect bond) has been a long-standing problem. The agreement found here between slow-combustion experiments with a columnar defect and the related ASEP model results indicates that this transition is indeed at a nonzero value of the respective control parameter. No scaling properties of the transition could be analyzed at this stage, but the ASEP model results also indicate that this transition is continuous. It remains an experimental and theoretical challenge to analyze this transition in more detail.

ACKNOWLEDGMENTS

The authors gratefully acknowledge support by the Academy of Finland (MaDaMe Program and Project No. 44875), and fruitful discussions with David Mukamel, Joachim Krug, and Mehran Kardar.

[1] M. Kardar, G. Parisi, and Y.-C. Zhang, Phys. Rev. Lett. **56**, 889 (1986).
[2] For a review, see, e.g., T. Halpin-Healy and Y.-C. Zhang, Phys. Rep. **254**, 215 (1995).
[3] V.K. Horváth, F. Family, and T. Vicsek, Phys. Rev. Lett. **67**, 3207 (1991).
[4] J. Maunuksela, M. Myllys, O.-P. Kähkönen, J. Timonen, N. Provatas, M.J. Alava, and T. Ala-Nissila, Phys. Rev. Lett. **79**, 1515 (1997); M. Myllys, J. Maunuksela, M.J. Alava, T. Ala-Nissila, and J. Timonen, *ibid.* **84**, 1946 (2000).
[5] M. Myllys, J. Maunuksela, M. Alava, T. Ala-Nissila, J. Merikoski, and J. Timonen, Phys. Rev. E **64**, 036101 (2001).
[6] R. Surdeanu, R.J. Wijngaarden, E. Visser, J.M. Huijbregtse, J. Rector, B. Dam, and R. Griessen, Phys. Rev. Lett. **83**, 2054 (1999).
[7] For an early similar observation, see V.K. Horváth, F. Family, and T. Vicsek, J. Phys. A **24**, L25 (1991).
[8] See also D. Forster, D.R. Nelson, and M.J. Stephen, Phys. Rev. A **16**, 732 (1977).
[9] J. Maunuksela, M. Myllys, J. Merikoski, J. Timonen, T. Kärkkäinen, M.S. Welling, and R.J. Wijngaarden, Eur. Phys. J. B **33**, 193 (2003).
[10] D.E. Wolf and L.-H. Tang, Phys. Rev. Lett. **65**, 1591 (1990).
[11] S.A. Janowsky and J.L. Lebowitz, Phys. Rev. A **45**, 618 (1992); J. Stat. Phys. **77**, 35 (1994).
[12] A.B. Kolomeisky, J. Phys. A **31**, 1153 (1998).
[13] D. Kandel and D. Mukamel, Europhys. Lett. **20**, 325 (1992).
[14] L.-H. Tang and I.F. Lyuksyutov, Phys. Rev. Lett. **71**, 2745 (1993).
[15] L. Balents and M. Kardar, Phys. Rev. B **49**, 13030 (1994).
[16] H. Kinzelbach and M. Lassig, J. Phys. A **28**, 6535 (1995).
[17] T. Hwa and Th. Nattermann, Phys. Rev. B **51**, 455 (1995).
[18] E.B. Kolomeisky and J.P. Straley, Phys. Rev. B **51**, 8030 (1995).
[19] M. Lassig, J. Phys.: Codens Matter **10**, 9905 (1998).
[20] M. Myllys, J. Maunuksela, J. Merikoski, and J. Timonen (unpublished).
[21] J.M. Burgers, *The Nonlinear Diffusion Equation* (Riedel, Boston, 1974).
[22] M. Ha, J. Timonen, and M. den Nijs, e-print cond-mat/0307403.
[23] F. Slanina and M. Kotrla, Physica A **256**, 1 (1998).

Circling the Square

Viktor K. Horváth
Department of Physics and Astronomy, University of Pittsburgh, Pittsburgh, PA 15260,
Eötvös University, Department of Biological Physics, H-1117 Budapest, Hungary.

"The symbol π [1] denotes the ratio of the circumference of a circle to its diameter. The ratio is approximately 3.14159265." (Encyclopedia Britannica, 1938)

I. INTRODUCTION

The history of π is a very interesting one and embraces almost the entire written human history. In the following some important results will be mentioned withouth the hope to provide a complete overview. Such an account was recently given for instance by Beckmann in his very interesting book on the history of π [2].

A good numerical approximation of π was already known by the people of ancient Egypt nearly 40 century ago. They used a numerical value of $256/81$ ($\simeq 3.16$) as a ratio of the circumference to the diameter [3], but we have no indication that they were aware that this value was only approximate rather than exact. Archimedes was the first who put scientific effort to compute the value of π [4]. Inscribing and circumscribing regular polygons he found that the value of π must be in the regime $[(3+10/71),(3+1/7)]$. We have learned from Lambert [5] and Lindemann [6] that the π is an irrational [7] number with transcendental [8] nature. Early in the 20th century the Indian mathematical genius Ramanujan developed several ways of calculating π. His series is so efficient that it has been incorporated into computer algorithms, permitting expressions of π in millions of digits. Ramanujan himself used the following numerical value as "sufficient" for practical applications: $63(17+15\sqrt{5})/25(7+15\sqrt{5})$=3.141592654....

The ghost of the "squaring the circle" arises in our computerized world in a new form. While people in the past used compass and rules to create their circles, the drawing tools of our modern life are the monitors of computers, the CCD sensors of video cameras, etc. These generally used devices have something in common, their 'paper' is a grid (or raster), i.e. a square lattice that is made of small squares (called pixels). In our computer age it is an everyday task to draw circles using squares (pixels) only and performing measurements on raster images. This article focuses on the later task in the most simple form, i.e. measuring the circumference of a digitized circle.

II. THE VALUE OF π ON A SQUARE LATTICE

Measuring some function along a circle (for instance a line integral, circulation of a velocity field, etc.) is a very common job in everyday scientific life. If the function is a constant identical to unity, then the result is the circumference of the circle. Therefore, it is fundamental issue to be able to precisely measure the circumference of a circle drawn on a lattice. This problem is identical to measuring π, i.e. the ratio of the circumference to the diameter.

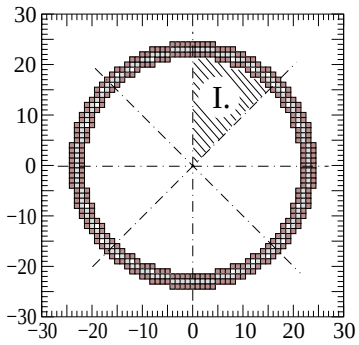

FIG. 1. Three circles drawn by gray and black pixels. The diameters (D=44,46, and 48) are measured in the units of pixels. Pixels for circles were assigned by calculating the position $Y=\sqrt{R^2-X_i^2}$ for each X_i, and choosing the coordinate Y_i that is closest to Y. Here $\{X_i, Y_i\}$ are the integer coordinates of pixel centers.

At first, one may assume that when walking along the continuous chain of pixels (i.e. the perimeter) one only needs to sum 1.0's and $\sqrt{2}$'s depending on if we step on nearest or second nearest neighbor pixel [10]. If we apply this simple counting method, we find that the circumference (i.e. the length of this particular pixel chain) is not precisely equal to πD. One can easily check in Figure 1 that for the circles with diameter 44,46, and 48 the measured circumference is 145.6 ($8*[9*1.0+6.5*1.41]$), 153.6 ($8*[10*1.0+6.5*1.41]$), and 159.2 ($8*[10*1.0+7*1.41]$) respectively. This compares to the expected (πD) values of 138.3, 144.5, and 150.8.

A typical misconception is to attribute the observed errors *only* to the small radius-to-pixel size ratio by implicitly assuming that increasing this ratio (by either increasing the diameter or decreasing the pixel size) will lead to a better approximation of the circumference. Figure 2 clearly demonstrates that the idea that the error in measuring π vanishes as the pixel size approaches zero is

simply wrong. The difference between the measured circumference C_m and the theoretically expected $C_t{=}\pi D$ increases with the diameter D. Using standard fitting procedure one finds that

$$C_m \simeq 1.0548 \cdot (\pi) D. \qquad (1)$$

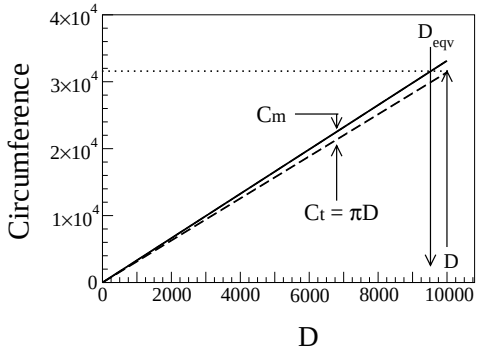

FIG. 2. The measured and the theoretical circumference versus the diameter D.

This result does *not* depend on the way we draw the circle. Although different circle drawing algorithms (midpoint, Breshenham's, etc.) may relocate some of the pixels, this will represent only a negligible difference, and won't change the value of C_m in large diameter limit. This can be perhaps best visualized in the following implicit manner. The linearly increasing difference between C_m and C_t (see Fig. 2) suggests that for a given circle of diameter D one can find another circle with an equivalent diameter $D_{eqv}(D)$ ($D_{eqv} < D$) that lead to a measured circumference equal to πD (i.e. $C_m(D_{eqv}){=}C_t(D)$). For a circle of diameter $D_1{=}10000$ the theoretically expected circumference is $C_t(D_1){=}31415.9$. From Eq. 1 one finds that $D_{eqv}{=}D/1.0548$, therefore $(D_1)_{eqv}{\simeq}9480$ (see Fig. 2). Obviously, 520 pixel difference between D and D_{eqv} cannot be accounted for by the (max.) ± 2 pixel uncertainty in the diameter caused by different circle drawing programs. This effect can be observed at small diameters too. In Fig. 1 the measured circumference ($C_m(D{=}44){=}145.6$) of a circle of diameter 44 was closer to the theoretical circumference of the circle of diameter 48 ($C_t(D{=}48){=}150.8$) than the measured value for the same circle ($C_m(D{=}48){=}159$).

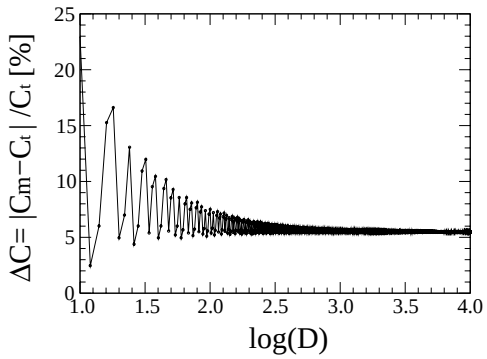

FIG. 3. Relative error versus the diameter of the circle. The diameter is measured in the unit of pixels.

The relative error of the measured circumference $\Delta C{=}|C_m - C_t|/C_t$ is shown in Figure 3. The upper envelope of this graph reveals the typical intuition, i.e. that the relative "error" decreases with increasing radius. However, one can see that ΔC asymptotically approaches to $\sim$5.4%, *not zero*.

Next, we look for the origin of this error. According to the introduction above, we only need to consider the first octant of the circle (see Fig. 1.). The circle starts right above the center and continues to the right. The first pixel is located above the center of the circle. (For simplicity we restrict the R values to integers only.)

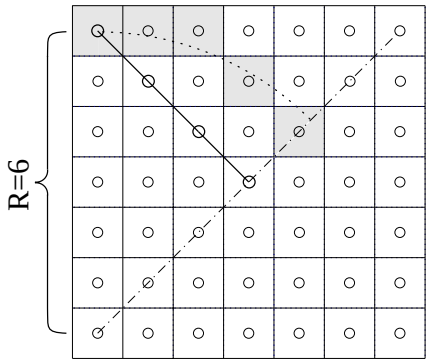

FIG. 4. Pixels with gray shadow represent the best approximation to the true arch shown by dotted line. Pixels that represent a badly approximated circle are connected by continuous line.

In this octant the slope of the perimeter changes from zero to -45^o, therefore the minimal possible arch is made by using only -45^o line segments (red line in Fig. 4). The length of this (red) perimeter segment is $R/\sqrt{2}$. However, this object is far from being part of a circle since along the diagonal (dashed line) the distance from the center to the red line is only $R/\sqrt{2}$ (and not R).

To better approximate a circle, one needs to shift the perimeter point along the diagonal further from the center. If this shift is only 1 pixel (as seen in Fig. 5), we change the circumference by $dC{=}2{-}\sqrt{2}$.

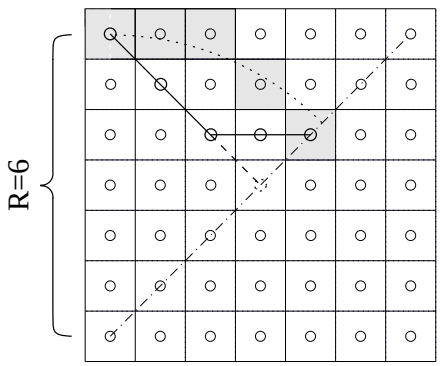

FIG. 5.

It is worth emphasizing that the value of dC does *not* depend on the actual path of the pixels. Pushing the perimeter along the diagonal by n instead of 1, the measured *total* circumference C_m is

$$C_m = 8(R/\sqrt{2} + n \cdot (2 - \sqrt{2})), \quad (2)$$

and the measured *radius* along the diagonal is

$$R_{diag} = R/\sqrt{2} + n\sqrt{2}. \quad (3)$$

Concerning the results in Figure 1, the relevant question is how much will the circumference increase if R_{diag}=R. This condition determines a specific value of n in Eq. 3

$$n^* = R \cdot \frac{\sqrt{2}-1}{2}. \quad (4)$$

Inserting n^* into Eq. 2 it follows that

$$C_m = \pi_\square D, \quad \text{where} \quad \pi_\square = 8(\sqrt{2}-1). \quad (5)$$

The numerical value of $\pi_\square$ ("square π") is ~ 3.31371, therefore if we write Eq. 5 in the form C_m=$(\pi_\square/\pi) * \pi D$, it is transparent that the ratio $\pi_\square/\pi$ ($\simeq 1.05478$) is in a perfect agreement with the pre-factor in Eq. 1.

III. HOW TO MEASURE THE CIRCUMFERENCE OF A CIRCLE?

The relative difference $(\pi_\square - \pi)/\pi$ (approx. 5.4%) is in good agreement with the measurement result shown in Figure 3. This is a surprisingly large discrepancy. For example, measuring the length of the Equator on a map with this 5.4% inaccuracy is equivalent to erasing the Danube river (the longest river in Central-Eastern Europe) from the map. Is there any way to minimize this error (and keep the river Danube on the map)? Fortunately the answer is yes.

The error in the previous measurements did not approach zero with decreasing mesh size. This is due to the fact that the "fine" mesh is not characterized *only* by the mesh size, but also by the number of possible angles of the line segments used to draw a circle. In the previous measurement there were only three different slopes available (0^o, 45^o, and 90^o) for line segments. This limited set of angles is not changed by decreasing the mesh size.

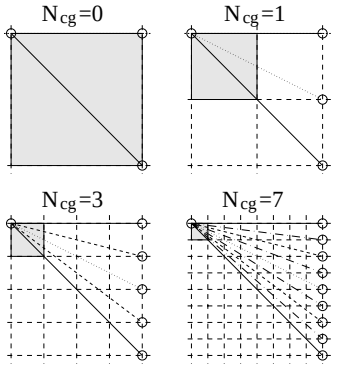

FIG. 6. The effect of increasing coarse grain number. Note that pictures with higher coarse grain number are shown with smaller magnification factor.

However, if we do not measure the distance between every subsequent pixel, but use only every odd pixel (omitting every even ones in the measurement), we *can* increase the number of possible angles between the two measurement points by one. Jumping over more than one pixel increases the variety of angles even further (see Fig. 6). The number of pixels omitted between two measurement points will be called the coarse grain number (N_{cg}).

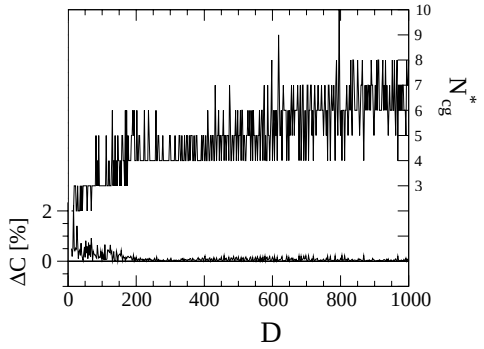

FIG. 7. The optimal coarse grain number versus the radius.

For a given circle of diameter D one can determine the optimal coarse grain number (N^*_{cg}), i.e. the one that minimizes the difference between the measurement results and the calculated πD. In measurements one finds that N^*_{cg} depends on the diameter as $N^*_{cg} \simeq 0.28 * \sqrt{D}$ (right axis Figure 7). In contrast to the previous measurements one finds that making measurements at $N^*_{cg}(D)$ the error approaches to zero at large diameter limit (left axis in Figure 7).

IV. THE OPTIMAL COARSE GRAIN NUMBER IN GENERAL

There are plenty of applications where line integrals are measured along an arbitrary line and not a circle. In general, one would like to measure the length using no a priori knowledge on the shape of the pixel chain. Is there any way to determine the optimal coarse grain number (and hence make precise measurements of the length) *without* using no extra information on the geometry?

A possible numerical solution is to measure the length (circumference for the circle) for several values of the coarse grain number, and take the $N_{cg} > 0$ value that provides the first *local* maxima for the relative error. This method was tested on 3 circles with different diameter. The results are shown in Fig. 9). One can see that starting with small N_{cg} the error rapidly decreases due to the increasing number of the possible different slopes. Then it stays close to zero for a certain range of the coarse grain number. This range depends on the radius.

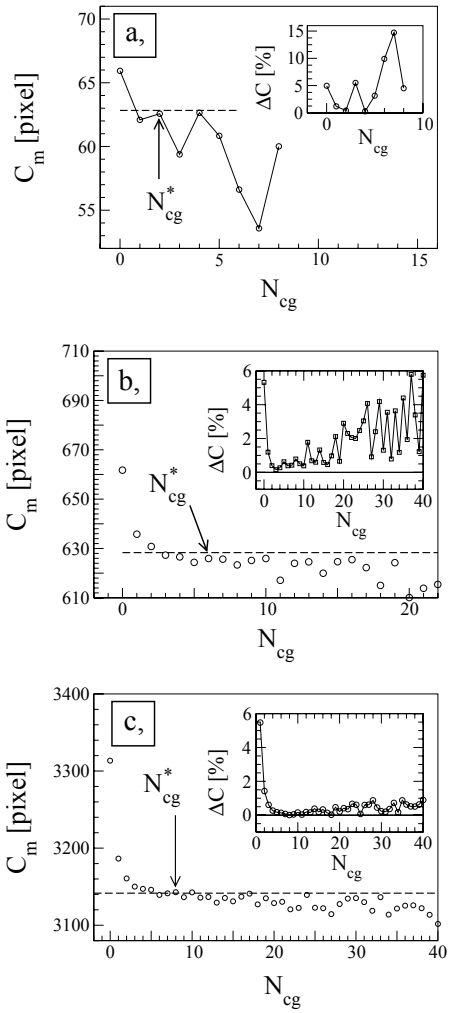

FIG. 8. The relative error versus coarse grain number for three circles with diameter D=20, 200, and 1000 respectively.

On the other side, if N_{cg} is too large then we begin to increase the error by approximating an arch by a straight line. An extreme example is when we jump over so many pixels that only four of them are left. In this case the measured circumference will be $4 * \sqrt{2}R$. This is clearly an *under*estimation of the true circumference.

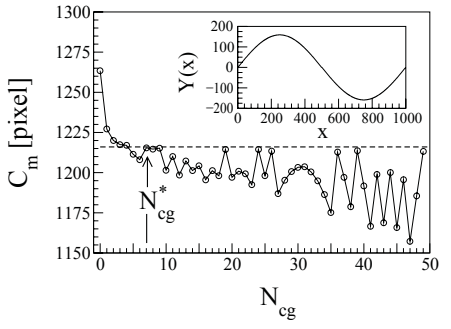

FIG. 9. Testing the corse grain method on arbitrary curve.

In general the optimal N^*_{cg} is determined by the first local maxima (shown by arrow in Fig. 9). In all cases N^*_{cg} determind by this method was in good agreement with the previous results seen in Fig. 7. In this test the diameter of the circles was kept constant and only N_{cg} was changed, therefore C_t remains the same. As a consequence, the measurement on C_m will show inflection point at values of N_{cg} where $|\Delta C|$ presents local maxima. If one cannot observe a characteristic inflection point in $C_m(N_{cg})$ then making an accurate measurement of length is hopeless.

Finally it is worth mentioning that this coarse grain method can also be useful in numerically solving any differential equation that contains spatial derivatives.

V. CONCLUSION

In order to be able to measure the circumference of a circle (or length of any pixel chain) with arbitrary precision, one needs to fulfill two conditions: First, the distance between two subsequent measurement points must be infinitely small. Second, the number of pixels between every two measurement points must be infinite. Only in this *dual limit* case will the true value of the circumference be revealed. In practice, measuring the circumference by stepping through all neighboring pixels only involves the first condition. To realize the important second condition, coarse graining must be implemented always. To determine the best coarse grain length for the most accurate measurement one needs to preform measurements at several values of the coarse grain number. Then the optimal value is either determined by observing an extended inflection point in the measurement or it is impossible to perform reliable measurement. Therefore, a good solver algorithm must require good resolution in the possible set of slopes too, and the above described coarse grained method provides a chance to accomplish this requirement.

Acknowledgment

I would like to thank to all my colleagues who patiently listened to the above puzzle. Special thanks goes to Walter Goldburg, Greg Huber, Béla Szilágyi and Matthew Shtrahman for their comments and careful reading of the manuscript. The author acknowledges support from OTKA T43122, M-27950, PFP-1168 and by NATO grant 9804461.

---

* Web: www.pitt.edu/∼vhorvath

[1] The symbol π was first used in 1706 by the English mathematician William Jones, but it became popular only after its adoption by the Swiss mathematician Leonhard Euler in 1737.

[2] Petr Beckmann, A History of π, 3rd ed., St. Martin's Press, New York, ISBN-0-312-38185-9 (1971).

[3] Rhind (or Ahmes) Papyrus, British Museum. In the "problem 50" the scribe recognized that the area of a circle is proportional to the square of the diameter and

assumed for the constant of proportionality (that is, $\pi/4$) the value 64/81. This extensive document from ancient Egypt has been the source of much information about Egyptian mathematics. The papyrus was copied at about 1650 BC (by Ahmes), and we know that it used a that time already 2 century old source. The papyrus earned its name from a Scottish antiquary, Alexander Henry Rhind, who discovered it in 1858.

[4] Around 200 BC, Archimedes of Syracuse reached a figure equivalent to about 3.14.

[5] Johann Heinrich Lambert (1728-1777), *Sechs Versuche einer Zeichenkunst in der Vernunftlehre* ("Six Attempts at a Symbolic Method in the Theory of Reason") (1777).

[6] Carl Louis Ferdinand von Lindemann (1852-1939), *Über die Zahl* π (11Concerning the Number π") (1882).

[7] By definition an irrational number cannot be expressed as a ratio of two whole numbers or as a decimal with a repeating pattern of digits.

[8] A transcendental number by definition cannot be the root of any algebraic or constructible equation with a *finite* number of terms.

[9] Among many algorithms that perform this simple task, perhaps Beshenham's algorithm is the best known. This very nice algorithm guarantees that 1, there are no holes along the perimeter; 2, every pixel is drawn only once; and 3, *only* linear operations are utilized (i.e. one avoids computing sin, cos, square or square-root). One can hardly expect more from an ideal circle algorithm.

[10] By definition "nearest neighbor" pixels share a side in contrast to "second nearest neighbors" that share only a corner (node).